IEEE Access
Multidisciplinary | Rapid Review | Open Access Journal

Received September 23, 2020, accepted October 11, 2020, date of publication October 14, 2020, date of current version October 26, 2020.

Digital Object Identifier 10.1109/ACCESS.2020.3030909

Analytical Modeling and Optimization Design of an Electromagnetic Pulse Welding Device With a Field Shaper for Metal Plates

HANG ZHANG, QINGJIAN WANG, GUANGDA WANG, (Member, IEEE), AND HONGFA DING, (Member, IEEE)

Wuhan National High Magnetic Field Center, Huazhong University of Science and Technology, Wuhan 430074, China

Corresponding author: Hongfa Ding (dhf@hust.edu.cn)

This work was supported in part by the National Key Research and Development Program of China under Grant 2016YFA0401702, and in part by the National Natural Science Foundation of China under Grant 51821005.

ABSTRACT An electromagnetic pulse welding (EMPW) system is a complex multifield coupling system. Using finite element software to simulate its processes can better guide the design of the electromagnetic pulse welding system and the analysis of the welding mechanism. However, the existing finite element software has a complex model, involves a large amount of calculation, and is time consuming, which is not conducive to the optimization of the welding device. In this paper, an equivalent circuit model based on an improved current wire method is proposed, and the welding process is modeled and analyzed, and then compared with the simulation results of the finite element software COMSOL. The results show that the analytical model is accurate and effective, and it can reduce the calculation time and improve the processing efficiency. Second, based on the equivalent circuit model and taking the maximum impulse of the electromagnetic force as the optimization objective, the shape parameters of the field shaper and the number of turns of the coil in the electromagnetic welding device for plates based on the field shaper are optimized, and the optimal parameters are obtained. Finally, the welding equipment is designed with the optimal parameters, and the electromagnetic welding platform is built. An SS304 stainless steel plate and A1060 aluminum plate with a thickness of 1 mm are welded, and the dissimilar metal plates are well connected.

INDEX TERMS Electromagnetic pulse welding, improved current wire method, equivalent circuit model, optimize, field shaper, maximum impulse, welding platform.

I. INTRODUCTION

With the development of the economy and of technology, vehicles are becoming increasing diversified. Energy saving and emission reduction methods have been given increasing attention [1]. Aluminum and its alloys have become the first choice for lightweight vehicles because of their good mechanical properties and low density [2]. When aluminum and its alloys are used in vehicles, they need to be connected with different metal plates. Electromagnetic pulse welding is a high-speed solid-state welding technology, which is of great significance in the welding of dissimilar metals [3]–[8].

The associate editor coordinating the review of this manuscript and approving it for publication was Pengcheng Liu.

An electromagnetic pulse welding system is a complex multifield coupling system, which involves circuits, heat, structures, electromagnetic fields and so on. Because the welding process is very short, it is difficult to collect and monitor the speed, stress and temperature of the welding process in real time. The existing simulation software can guide the design of electromagnetic pulse welding systems and the analysis of welding mechanisms [9].

Aizawa [10] calculated the electromagnetic force on an improved single-turn coil. The calculation method is based on the Lorentz force formula. The calculation method is simple, but it ignores the influence of the skin effect, and the accuracy of the calculation is not high. Yu and Tong [11] used the loose coupling mode of the electromagnetic field module and structural field module in ANSYS finite

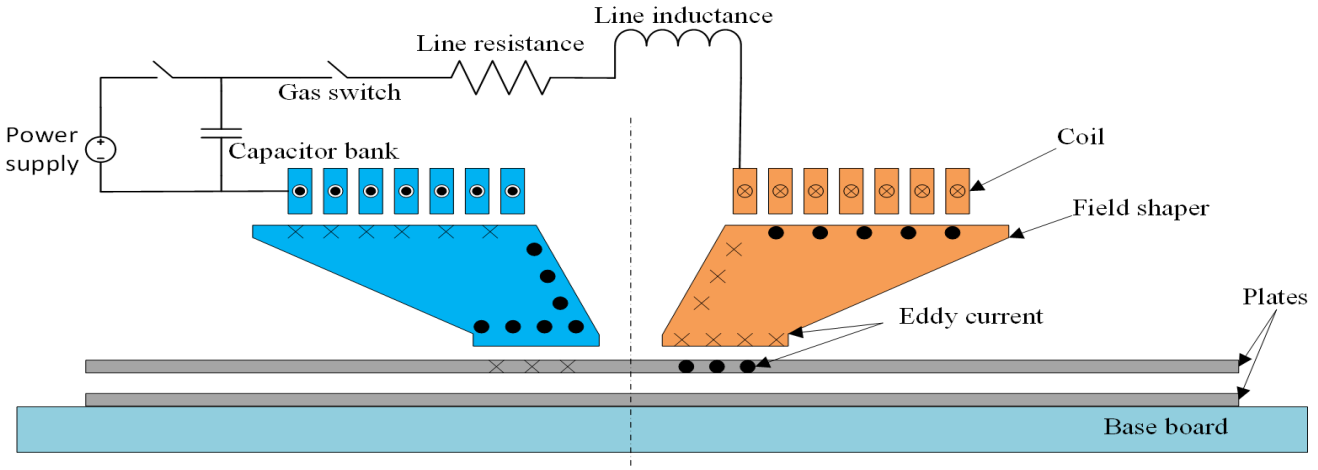

FIGURE 1. Schematic diagram of the electromagnetic pulse welding system.

element software to optimize the shape of a field shaper, and tried to determine the influence of the field shaper on magnetic pressure during the welding process. Kore *et al.* [12]–[14] used ANSYS to simulate the electromagnetic field in the welding process, calculated the electromagnetic force at different times for the workpiece node, and then imported it into ABAQUS to simulate the welding collision process, achieving the loose coupling of the electromagnetic field and structural field. Hisashi *et al.* [15] used the commercial finite element software MSC Dytran to numerically simulate the temperature and stress distribution of Al-Fe plate welding and then obtained a sequential coupling simulation of the temperature field and structure field. Fan *et al.* [16] used ANSYS to analyze the electromagnetic force in the welding process. The electromagnetic force was introduced into LSDYNA, and the smoothed particle hydrodynamics (SPH) method was used to simulate the welding process.

From the existing research, it can be seen that the existing numerical simulations of electromagnetic pulses are mainly based on commercial finite element software, and some of them are obtained by numerical calculation [17]. The input of the simulation is the measured current curve or the current curve obtained by other software simulations, so a coupling analysis of the electromagnetic welding and discharge circuit is rarely found [18]; the model is complex, and the calculation is large and time consuming. In this paper, an equivalent circuit model based on an improved current wire method is proposed. The electromagnetic coupling between components is considered in the model. By coupling the discharge circuit to the electromagnetic pulse welding process, the calculation accuracy can be improved. The calculation of the equivalent circuit model is simpler, which can reduce the calculation time and improve the processing efficiency [19], [20]. In this paper, the virtual displacement method is used to solve the axial electromagnetic force, and the electromagnetic force is integrated on the time axis to obtain the impulse within a time t. Based on this method, the welding device is optimized and the welding experiment is carried out.

II. ESTABLISHMENT OF AN EQUIVALENT CIRCUIT MODEL

The EMPW system with a field shaper mainly includes a charging system, a capacitor bank, a discharge switch, a driving coil, a field shaper and plates as shown in the schematic diagram of Fig. 1. The capacitor discharges the coil to generate a magnetic field, and the field shaper placed between the coil and the plate causes the magnetic field to converge so that the large Lorentz force in the welding area drives the flying board at high speed to hit the parent plate to achieve welding. To optimize the design of the field shaper and coil in the welding device, it is necessary to accurately determine the basic parameters such as the voltage, current and electromagnetic force in the process of EMPW. To obtain accurate results, the electromagnetic coupling between the model components should be considered. In this paper, the equivalent circuit model based on the current wire method is used to represent the welding device equivalently. This method takes into account the electromagnetic coupling between the components; it uses the analytical method to calculate, and the calculation efficiency is high.

A. PRINCIPLE OF EQUIVALENT MODELS

The core idea of the equivalent circuit method is to establish a circuit model equivalent to the electromagnetic field. The premise of its application is that the model is axisymmetric and is transformed into a two-dimensional axisymmetric model during modeling. A non-axisymmetric model cannot be calculated by the current wire method. The coil and plates in the electromagnetic pulse welding device based on the field shaper are two-dimensional axisymmetric models. The physical structure of the field shaper is shown in Fig. 2. Due to the existence of the gap, the field shaper is a non-axisymmetric component, and the existing equivalent circuit model cannot be used for calculation. To make use of the current wire

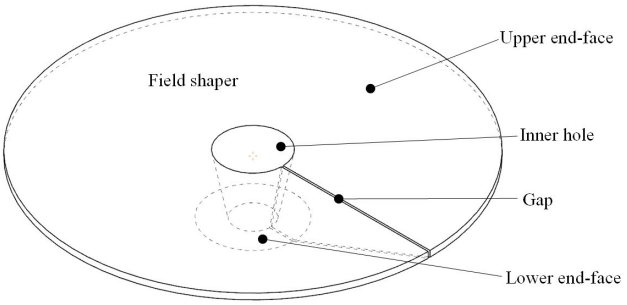

FIGURE 2. Physical structure of the field shaper.

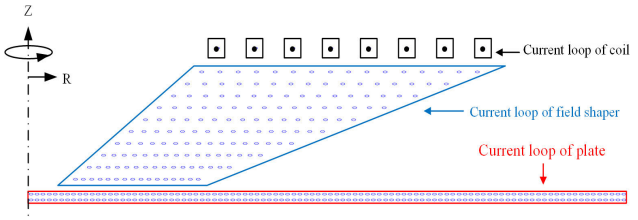

FIGURE 3. Discretization of welding equipment.

method for analysis, according to the working principle of the field shaper, the following approximate assumptions are made for the field shaper:

1) The current passing through any section of the axis of the inner hole of the field shaper is zero.
2) The voltage of any section passing through the axis of the inner hole of the field shaper is equal everywhere.

Except for the cross-section near the gap of the field shaper, all positions satisfy these assumptions. Based on the assumptions, the electromagnetic system can be considered equivalent to a two-dimensional axisymmetric model.

In the model, the coil, field shaper and plate are separated into a series of coaxial current wire rings with small diameters. The resistance, inductance and mutual inductance of the current wires are considered in the calculation. The equivalent models of the coil, collector and plate are shown in Fig. 3. In the figure, each turn of the coil is treated intensively, which is equivalent to a current wire. The field shaper and the plate are divided into multiple current wires. The current wire in the Z direction is fixed at 10 layers, and the current wire in the R direction has 2 coil turns. The current wire spacing in the Z and R directions of the plate is 0.5 mm. The higher the density of the current wire is, the higher the calculation accuracy will be, but the amount of calculation will also increase and the time consumption will increase.

B. EQUIVALENT CIRCUIT AND EQUATION

The coil, field shaper and plate system shown in Fig. 3 can be considered equivalent to the circuit model shown in Fig. 4. The coupling between the coil and the field shaper and between the field shaper and the plate is conducted by an electromagnetic field. Due to the long distance between the plate and the coil, and because the field shaper plays a

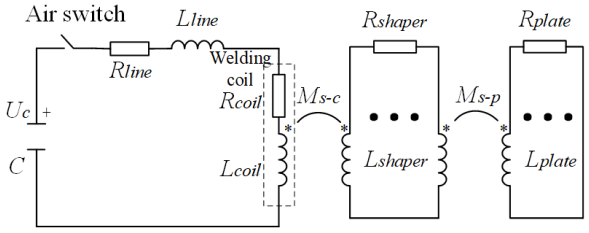

FIGURE 4. Equivalent circuit model of the EMPW.

TABLE 1. Meaning of the symbols in the equations.

Symbol	Meaning	Symbol	Meaning
R_L	Equivalent resistance of the line	L_C	Equivalent inductance of the coil
L_L	Equivalent inductance of the line	u_c	Capacitance voltage
R_S	Equivalent resistance of the field shaper	u_s	Field shaper current loop voltage
L_S	Equivalent inductance of the field shaper	i_c	Line current
R_P	Equivalent resistance of the plate	i_s	Field shaper current loop current
L_P	Equivalent inductance of the plate	i_p	Plate current loop current
R_C	Equivalent resistance of the coil	$M_{i\text{-}j}$	Current loop mutual inductance

shielding role in the process of electromagnetic energy transfer, the coupling between the plate and the coil is ignored. According to the relationship among the resistance, self-inductance and mutual inductance of each current wire, a series of differential equations can be obtained as shown below. By solving the differential equations, the current value of each current wire over time can be obtained. The meaning of the symbols in the formula group is shown in Table 1.

$$i_c = -C\frac{du_c}{dt} \tag{1}$$

$$i_c R_L + L_L\frac{di_c}{dt} + i_c R_c + L_c\frac{di_c}{dt} + \sum_{s=1}^{j} M_{s-c}\frac{di_s}{dt} = u_c \tag{2}$$

$$i_s R_s + L_s\frac{di_s}{dt} + \sum_{\substack{r=1\\ r\neq s}}^{j} M_{s-r}\frac{di_s}{dt} + M_{s-c}\frac{di_c}{dt} + \sum_{p=1}^{k} M_{s-p}\frac{di_p}{dt} = u_s \tag{3}$$

$$\sum_{s=1}^{j} i_s = 0 \tag{4}$$

$$i_p R_p + L_p\frac{di_p}{dt} + \sum_{\substack{r=1\\ r\neq p}}^{k} M_{p-r}\frac{di_p}{dt} + \sum_{s=1}^{j} M_{p-s}\frac{di_s}{dt} = 0 \tag{5}$$

Eq. (1) represents the capacitance discharge equation. Eq. (2) represents the coil discharge equation, in which the coil resistance and inductance and the mutual inductance between the coil and the single current loop of the field shaper are replaced by centralized parameters. The formula is as follows:

$$L_c = \sum_{i=1}^{n} L_i \tag{6}$$

$$M_{s-c} = M_{c-s} = \sum_{i=1}^{n} M_{s-i} \tag{7}$$

$$R_c = \sum_{i=1}^{n} R_i \tag{8}$$

Eq. (3) represents the circuit equation of a single current filament loop in the magnetic concentrator. Eq. (4) indicates that the sum of the current on the cross-section of the collector is zero. Eq. (5) is the circuit equation of a single current loop in the plate.

C. PARAMETERS OF THE EQUIVALENT MODEL

In the above equations, the known parameters are the line inductance resistance, energy storage capacity and initial voltage, and the required solution is the coil current and the current of each current wire of the field shaper and the plate. To obtain these parameters, it is necessary to calculate the resistance, self-inductance and mutual inductance of each current wire.

Eq. (9) is the resistance formula for each current ring, where ρ is the resistivity of the device material, r is the radius of the current wire loop, and a is the equivalent cross-sectional area of each current wire ring. Eq. (10) is the self-inductance formula of each current wire ring, where μ_0 is the vacuum permeability and d_{eq} is the diameter of the equivalent cross-section of each current wire ring. The size is shown in Eq. (11).

$$R = \rho \frac{2\pi r}{a} \tag{9}$$

$$L = \mu_0 r \left(\ln \left(\frac{16r}{d_{eq}} \right) - \frac{7}{4} \right) \tag{10}$$

$$d_{eq} = 2\sqrt{\frac{a}{\pi}} \tag{11}$$

Eq. (12) is the mutual inductance between the two current loops, r_i and r_j are the radii of the two current loops, z_i and z_j are the Z coordinates of the two current rings, and k is the correlation function of the above parameters.

$$M_{ij} = \mu_0 \sqrt{r_i r_j} \left(\left(\frac{2}{k} - k \right) K(k) - \frac{2}{k} E(k) \right) \tag{12}$$

$$k = \mu_0 \sqrt{\frac{4 r_i r_j}{\left(r_i + r_j\right)^2 + \left(z_i - z_j\right)^2}} \tag{13}$$

where K(k) and E(k) are complete elliptic integrals of type 1 and type 2 respectively, and their specific expressions are given by the following equations:

$$K(k) = \int_0^1 \frac{d_t}{\sqrt{\left(1 - t^2\right)\left(1 - k^2 t^2\right)}} \tag{14}$$

$$E(k) = \int_0^1 \frac{\sqrt{1 - k^2 t^2}}{\sqrt{1 - t^2}} d_t \tag{15}$$

To calculate the current of each current wire, it is necessary to solve several equations. The number of equations is determined by the number of current wires and Eqs. (1) - (5). To better understand and solve the equations, they are expressed in the form of a matrix and are solved by MATLAB. The matrix form of the differential equations is shown in Eq. (16).

$$\begin{bmatrix} \frac{d\boldsymbol{I}}{dt} \\ \frac{dU_c}{dt} \end{bmatrix} = \begin{bmatrix} -\boldsymbol{L}^{-1}\boldsymbol{R} & \boldsymbol{L}^{-1}\boldsymbol{E} \\ -\boldsymbol{L}^{-1}\boldsymbol{C} & X \end{bmatrix} \begin{bmatrix} \boldsymbol{I} \\ U_c \end{bmatrix} \tag{16}$$

The matrix equation primarily describes the relationship among the voltage, current, resistance, inductance and mutual inductance of each current wire. The current matrix, resistance matrix, capacitance matrix and inductance matrix of the current wire are expressed as follows:

$$\boldsymbol{I} = \left[i_L, i_{s1}, \ldots, i_{sj}, i_{p1}, \ldots, i_{pk} \right]^T \tag{17}$$

$$\boldsymbol{R} = \begin{bmatrix} R_c & 0 & 0 \\ 0 & R_s & 0 \\ 0 & 0 & R_p \end{bmatrix} \tag{18}$$

$$\boldsymbol{C} = \begin{bmatrix} \frac{1}{C}, & 0, & \ldots & 0 & 0 \\ 0 & 1, & \ldots . & 1 & 1 \end{bmatrix} \tag{19}$$

$$\boldsymbol{L} = \begin{bmatrix} LM_c & M_{c-s} & M_{c-p} \\ M_{s-c} & LM_s & M_{s-p} \\ M_{p-c} & M_{p-s} & LM_p \end{bmatrix} \tag{20}$$

where LM_c represents the self-inductance and mutual inductance of each current wire of the coil, LM_s represents the self-inductance and mutual inductance of each current wire of the field shaper, and LM_p represents the self-inductance and mutual inductance of each current wire of the plate. The above matrix can be obtained from Eqs. (9) - (15).

III. MODEL VALIDATION

To verify the correctness of the equivalent circuit model, the equivalent circuit method and finite element method are used to calculate with the same parameters. The set conditions are as follows: the discharge voltage is 10 kV, the capacitance value is 100 μF, the external inductance is 1.5 μH, the external resistance is 50 mΩ, and the number of coil turns is 8. The sizes of the field shaper and coil are consistent with the optimization parameters in Section 4.

Fig. 5 shows a comparison between the discharge current curve calculated by the finite element method and the equivalent circuit method and the current curve measured by experiment. Since the main function of welding is in the first current pulse, only the first pulse is taken. It can be seen from

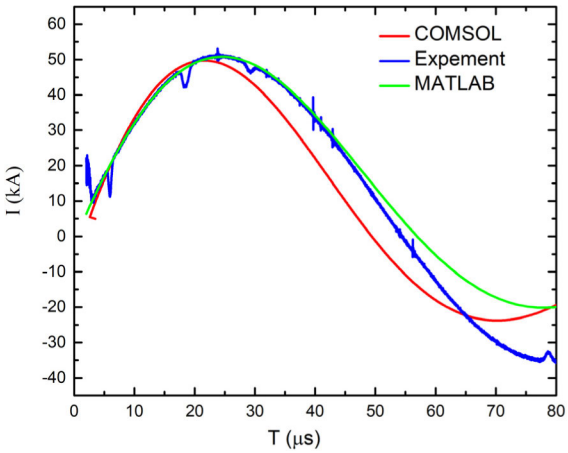

FIGURE 5. Comparison of the current curves.

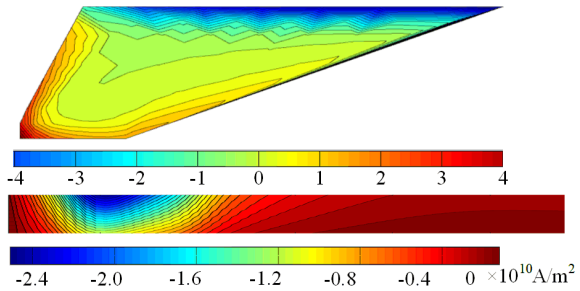

FIGURE 6. Current distribution nephogram calculated by the equivalent circuit method.

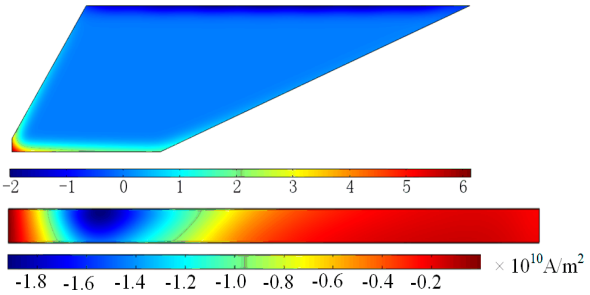

FIGURE 7. Current distribution nephogram calculated by COMSOL.

the figure that the three current waveforms are well matched, which meets the analysis requirements of electromagnetic pulse welding.

Figs. 6 and 7 show the current distribution nephogram at the maximum current moment calculated by the equivalent circuit method and the finite element method, respectively. The figure shows that the current distribution nephogram calculated by the equivalent circuit method is in good agreement with that calculated by the finite element method. However, there are also differences. The main reason for this is that the current wire density of the equivalent circuit method is less than the cell density of the finite element method.

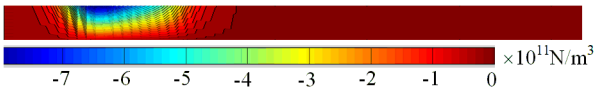

FIGURE 8. Electromagnetic force distribution nephogram calculated by the virtual displacement method.

By solving the equivalent circuit equation, the coil discharge current and the eddy current of the field shaper and the plate can be obtained. Based on the principle of electromagnetic energy storage, the total energy storage of the electromagnetic system can be obtained, as shown in Eq. (21). In this paper, the virtual displacement method is used to determine the axial electromagnetic force. By deriving the magnetic energy in the Z direction, the axial electromagnetic force on the current ring of the plate can be obtained, as shown in Eq. (22).

$$\begin{aligned} W_M &= \frac{1}{2}(L_c I_c + \sum_{s=1}^{j} M_{c-s} i_s) I_m \\ &\quad + \sum_{s=1}^{j} \frac{1}{2}(L_s i_s + M_{s-c} I_c + \sum_{r=1, r\neq s}^{j} M_{r-s} i_s + \sum_{p=1}^{k} M_{s-p} i_p) i_s \\ &\quad + \sum_{p=1}^{k} \frac{1}{2}(L_p i_p + \sum_{p=1, r\neq p}^{k} M_{r-p} i_p + \sum_{s=1}^{j} M_{p-s} i_p) i_p \quad (21) \\ F_p^z &= \frac{\partial}{\partial z_p} W_M \\ &= \frac{1}{2} i_p^2 \frac{\partial}{\partial z} L_p + \sum_{\substack{r=0 \\ r\neq p}}^{k} i_p i_r \frac{\partial}{\partial z} M_{p-r} + \sum_{s=0}^{j} i_p i_s \frac{\partial}{\partial z} M_{p-s} \\ &= \sum_{\substack{r=0 \\ r\neq p}}^{k} i_p i_r \frac{\partial}{\partial z} M_{p-r} + \sum_{r=0}^{j} i_p i_s \frac{\partial}{\partial z} M_{p-s} \quad (22) \end{aligned}$$

where the first term is the electromagnetic force generated by the magnetic field of the plate ring p, which only has a radial force component, which is ignored when calculating the Z-direction force; the second term is the electromagnetic force exerted by the other current rings of the plate on the current ring p; and the third term is the electromagnetic force generated by the field shaper on the plate ring p.

Figs. 8 and 9 show the cloud charts of the electromagnetic force distribution of the plate in the Z-direction obtained by the virtual displacement method and finite element method, respectively. The figure shows that the electromagnetic force is mainly concentrated at the position of the lower end-face of the field shaper, and the two agree well, but the electromagnetic force calculated by the virtual displacement method is slightly larger because the air energy storage is ignored in the calculation.

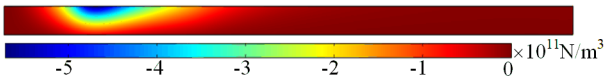

FIGURE 9. Electromagnetic force distribution nephogram calculated by COMSOL.

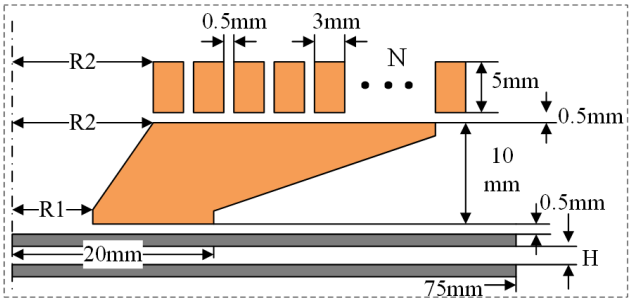

FIGURE 10. Structure and size of the welding device.

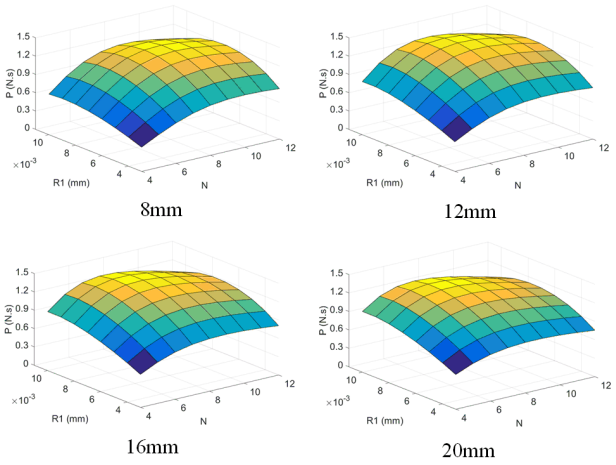

FIGURE 11. Electromagnetic force impulse of the welding area under different coil inner radius.

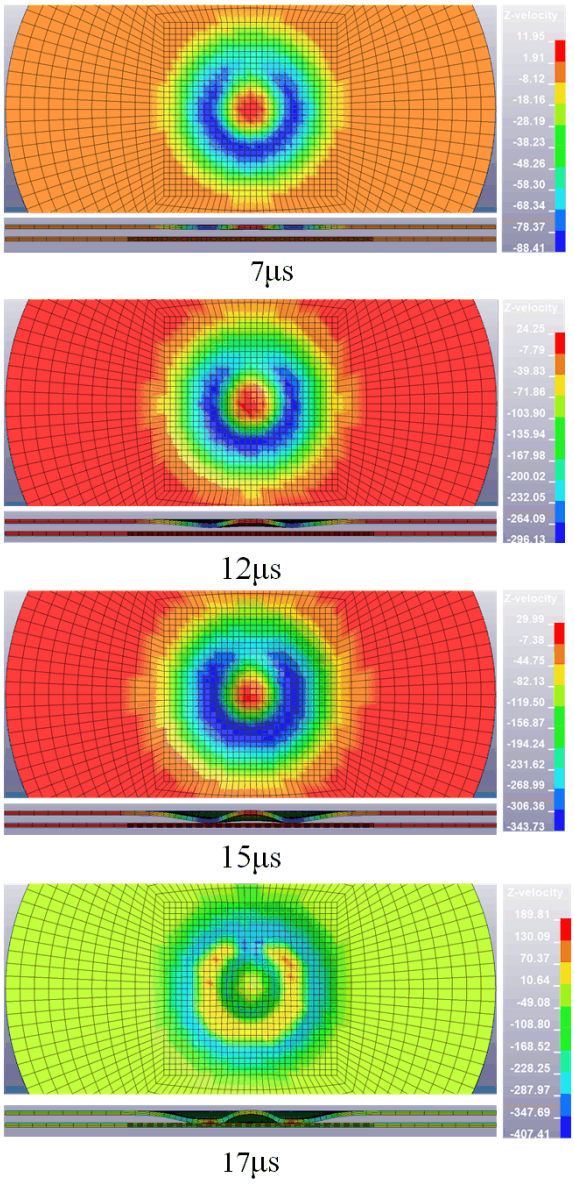

FIGURE 12. Electromagnetic pulse welding equipment.

From the above current distribution nephogram, it can be seen that the current distribution of the field shaper and the plate are in good agreement, which shows that the equivalent circuit method can meet the design requirements and has high accuracy. Moreover, the distribution of the electromagnetic force can also reflect the real distribution of the electromagnetic force, which provides the conditions for subsequent optimization.

IV. OPTIMIZATION OF WELDING EQUIPMENT

The EMPW system includes the welding power supply, coil and field shaper. In this paper, the existing power supply system of the laboratory is used for the power supply, and only the field shaper and coil are optimized. The structure and size of the welding device are shown in Fig. 10. The outer diameter of the lower end of the field is determined by the welding area, and the fixed radius used in this paper is 20 mm. For the thickness of the field shaper, a thickness greater than 2 times the skin depth is theoretically sufficient, but to ensure the strength of the field shaper, the thickness is fixed at 10 mm. The main parameters that affect the magnetic field and eddy current at the end of the field shaper are the number of coil turns, the radius of the upper end of the inner hole (inner radius of the coil) and the radius of the lower end of the inner hole. When the other parameters are fixed, this paper optimizes only the number of coil turns N, the radius of the upper end of the inner hole R2 (coil radius) and the radius of the lower end of the inner hole R1. In this section, the equivalent circuit model established above is used for parameter optimization, automatic parameter scanning is performed by the software, and the results are stored. The time

consumption is short, which is conducive to the optimization design.

In the equivalent circuit method, the velocity at the time of collision cannot be obtained directly, but the Lorentz force of each time step can be obtained. Therefore, the equivalent circuit method is used to calculate the electromagnetic force in the welding area, and the electromagnetic force is integrated on the time axis to obtain the impulse within time t. The optimization goal is to maximize the impulse of the electromagnetic force P. Because a distance between the plates of 1 mm to 2 mm is the most reasonable, the collision speed of electromagnetic welding is generally greater than 300 m/s, and the movement time t of the plate is approximately 10 μs after calculation.

According to the existing welding equipment parameters, the optimized voltage is 10 kV, the line inductance is 1.5 μH and the circuit resistance is 50 mΩ. The coil wire is made of red copper wire, and the field shaper is made of Cu-Cr-Zr. The size is shown in Fig. 10. In this optimization process, the inner radius of the coil is fixed first, and then the coil turns and the inner radius of the lower end of the field shaper are scanned. The electromagnetic force impulse in the welding area of the sheet metal is recalculated with each parameter change. The optimized parameters of the welding device are the number of turns, the inner radius of the field shaper and the inner radius of the coil at the maximum impulse. Fig. 11 shows the relationship between the electromagnetic force impulse of the welding area of the plate, the inner radius of the lower end of the field shaper and the number of coil turns when the coil inner radius is 8 mm, 12 mm, 16 mm and 20 mm.

Fig. 11 shows that the impulse distribution of the electromagnetic force in the four cases follows the same law; the maximum point appears at 8 turns of coil and 8 mm of the inner hole radius at the lower end of the field shaper, which is the optimal value of the parameter. It can also be seen from Fig. 11 that the inner radius of the coil has little effect on the impulse within a certain range. Considering the processing of the coil and the mechanical strength of the field shaper, the inner radius of the coil is determined to be 16 mm in this design.

V. ANALYSIS OF THE PLASTIC DEFORMATION PROCESS OF THE PLATE

Based on the optimization results, this paper establishes a three-dimensional finite element model to analyze the macroscopic plastic deformation process in welding via LS-DYNA. Fig. 12 describes the entire process for the aluminum plate from the beginning of the movement to the completion of high-speed collision welding under the action of the electromagnetic force. In the process of macroscopic plastic deformation, the discharge voltage is 10 kV, the pre-welding gap is 2mm, and the duration of this process is approximately 18 μs.

The deformation of the aluminum plate in the figure shows the electromagnetic pulse welding process can be roughly divided into the following four steps:

1) The 1-7 μs stage has a long duration, and the speed of the workpiece at this stage is low. The main reason is that the current density and magnetic field of the eddy current in the workpiece are small, the electromagnetic force is small and the acceleration is small. At this stage, the displacement of the workpiece is small, and it is basically in an undeformed state.
2) In the 7-12 μs stage, due to the large electromagnetic force on the plates during this period, the acceleration of the aluminum plate is obviously increased, and the maximum speed is increased to 296 m/s. It can also be seen from the figure that the speed and displacement of the area corresponding to the inner hole of the field shaper are relatively small, and the plate shows obvious deformation.
3) In the 12-15 μs stage, the aluminum plate further accelerates to 343 m/s, and the two plates are about to collide. As seen in the figure, the displacement of the position corresponding to the inner hole of the field shaper remains unchanged, with almost no speed or displacement.
4) In the 15-17 μs stage, the aluminum plate collides with the stainless steel plate. The collision starts from the fastest point and then extends to other positions. During the expansion of the collision range, there will be different collision angles between the plates. The location of the collision is concentrated in the area corresponding to the lower end of the field shaper, and the position corresponding to the inner hole of the field shaper hardly deforms at all. This is because the magnetic field and electromagnetic force in this area are small and are not sufficient to push the plate into collision.

From the analysis of the macroscopic plastic deformation process, it can be seen that in the electromagnetic pulse welding based on the field shaper, the aluminum plate with better conductivity undergoes severe plastic deformation, and the deformation position just corresponds to the distribution of electromagnetic force analyzed above, while the stainless steel plate, with poor conductivity, shows almost no deformation. Since the collision process of the workpiece is short and the grid cell size is large, only the collision area and velocity distribution can be roughly analyzed from a macro perspective.

VI. EXPERIMENT AND DISCUSSION

In this paper, the welding equipment is designed with the optimized parameters, and the electromagnetic welding platform is built. The equipment used in the experiment is presented in Fig. 13, including a power supply of 200 kJ, a capacitor bank of 100 μF with a peak voltage of 15 kV, the welding device, and the plates. The welding device is composed of a coil, field shaper and stainless steel tray fixed by an epoxy plate and bolt. The coil, field shaper and tray are shown in Fig. 14.

FIGURE 13. Electromagnetic pulse welding equipment.

FIGURE 14. Coil, field shaper and stainless steel tray.

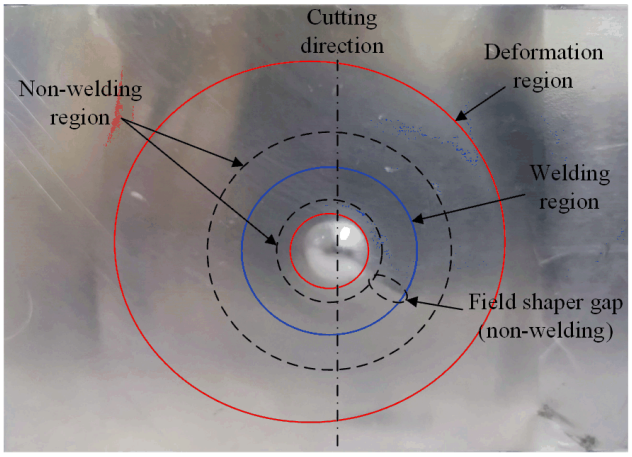

FIGURE 15. Appearance of the welding sample.

An SS304 stainless steel plate and A1060 aluminum plate with a thickness of 1 mm were welded under a 10 kV discharge voltage with a 2 mm pre-welding gap. The appearance of the welding sample is shown in Fig. 15. The deformation region of the plate coincides with the lower contour of the field shaper. The raised area corresponds to the center hole of the field shaper. The welding area is located on the periphery of the raised area. The non-welding area is divided into two main parts; one is between the convex area and the welding area and outermost region, and the other part corresponds to the gap in the field shaper. The welding device completes

FIGURE 16. Section of the welding sample.

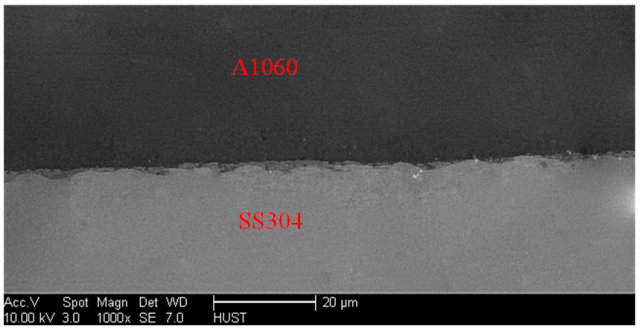

FIGURE 17. Microstructure of the welding joint.

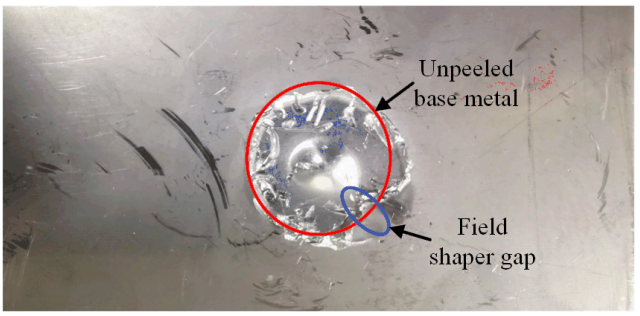

FIGURE 18. Peel test of the welding sample.

the local welding of the steel plate. To obtain the a clear welding area of the the welding sample, a section analysis of the welding sample is carried out in this paper. The cutting direction of the interface is shown in Fig. 15. In Fig. 16, we can clearly see the bulge in the center of the deformation zone in Zone A, and the welding between Zones B and C is good.

Macroscopically, both Zone B and Zone C in Fig. 16 are good welding zones. To better observe the microstructure of the welding area, we used a scanning electron microscope to enlarge it, as shown in Fig. 17. A relatively complete wavy interface is formed between the plates in the welding area. This shows that the welding area is fully engaged. To further evaluate the strength of the welded joint, a mechanical clamp was used to peel off the welding sample. Fig. 18 shows that the welding area cannot be peeled off, indicating that the strength of the welded joint is greater than that of the metal plate; the results show that the strength of the welded joint can meet the requirements of application, which verifies the strength of the welded joint.

VII. CONCLUSION

In this paper, the equivalent circuit model of an electromagnetic pulse welding device is established to solve the problem of electromagnetic coupling between the components. The welding device is optimized by using the equivalent circuit

method, and a welding platform is built and verified by experiments. Finally, the following conclusions are drawn:

1) The equivalent circuit model is used in the coupling analysis of the electromagnetic welding and discharge circuit, and it can effectively reflect the distribution of the current and electromagnetic force in the welding process.
2) The equivalent circuit model is helpful in better understanding the nature of the electromagnetic effect of electromagnetic pulse welding. It can reduce the calculation time, improve the processing efficiency and meet the design requirements of the welding equipment.
3) When the welding area is fixed, the equivalent circuit model can make the optimization of the welding device simple and efficient.
4) By optimizing the welding platform, the effective welding of dissimilar metal plates can be achieved.

REFERENCES

[1] L. Qiu, Y. Li, Y. Yu, A. Abu-Siada, Q. Xiong, X. Li, L. Li, P. Su, and Q. Cao, "Electromagnetic force distribution and deformation homogeneity of electromagnetic tube expansion with a new concave coil structure," *IEEE Access*, vol. 7, pp. 117107–117114, 2019, doi: 10.1109/ACCESS.2019.2923264.

[2] V. Psyk, D. Risch, B. L. Kinsey, A. E. Tekkaya, and M. Kleiner, "Electromagnetic forming—A review," *J. Mater. Process. Technol.*, vol. 211, no. 5, pp. 787–829, 2011, doi: 10.1016/j.jmatprotec.2010.12.012.

[3] R. Qiu, C. Iwamoto, and S. Satonaka, "Interfacial microstructure and strength of steel/aluminum alloy joints welded by resistance spot welding with cover plate," *J. Mater. Process. Technol.*, vol. 209, no. 8, pp. 4186–4193, Apr. 2009, doi: 10.1016/j.jmatprotec.2008.11.003.

[4] A. Kapil and A. Sharma, "Magnetic pulse welding: An efficient and environmentally friendly multi-material joining technique," *J. Cleaner Prod.*, vol. 100, pp. 35–58, Aug. 2015, doi: 10.1016/j.jclepro.2015.03.042.

[5] M. Kimchi, H. Shao, W. Cheng, and P. Krishnaswamy, "Magnetic pulse welding aluminium tubes to steel bars," *Weld. World*, vol. 48, nos. 3–4, pp. 19–22, Mar. 2004, doi: 10.1007/BF03266422.

[6] L. Qiu, K. Deng, A. Abu-Siada, Q. Xiong, N. Yi, Y. Fan, J. Tian, and J. Jiang, "Construction and analysis of two-dimensional axisymmetric model of electromagnetic tube bulging with field shaper," *IEEE Access*, vol. 8, pp. 113713–113719, 2020, doi: 10.1109/ACCESS.2020.3003740.

[7] A. P. Manogaran, P. Manoharan, D. Priem, S. Marya, and G. Racineux, "Magnetic pulse spot welding of bimetals," *J. Mater. Process. Technol.*, vol. 214, no. 6, pp. 1236–1244, Jun. 2014, doi: 10.1016/j.jmatprotec.2014.01.007.

[8] H. Zhang, N. Liu, X. Li, F. Deng, Q. Wang, and H. Ding, "A novel field shaper with slow-varying central hole for electromagnetic pulse welding of sheet metal," *Int. J. Adv. Manuf. Technol.*, vol. 108, nos. 7–8, pp. 2595–2606, Jun. 2020, doi: 10.1007/s00170-020-05454-z.

[9] J. Lueg-Althoff, J. Bellmann, S. Gies, S. Schulze, A. E. Tekkaya, and E. Beyer, "Influence of the flyer kinetics on magnetic pulse welding of tubes," *J. Mater. Process. Technol.*, vol. 262, pp. 189–203, Dec. 2018, doi: 10.1016/j.jmatprotec.2018.06.005.

[10] T. Aizawa, "Magnetic pressure seam welding method for aluminium sheets," *Weld. Int.*, vol. 17, no. 12, pp. 929–933, Dec. 2003, doi: 10.1533/wint.2003.3199.

[11] H. Yu and Y. Tong, "Magnetic pulse welding of aluminum to steel using uniform pressure electromagnetic actuator," *Int. J. Adv. Manuf. Technol.*, vol. 91, nos. 5–8, pp. 2257–2265, Jul. 2017, doi: 10.1007/s00170-016-9928-y.

[12] S. D. Kore, P. Dhanesh, S. V. Kulkarni, and P. P. Date, "Numerical modeling of electromagnetic welding," *Int. J. Appl. Electromagn. Mech.*, vol. 32, no. 1, pp. 1–19, Jan. 2010, doi: 10.3233/JAE-2010-1062.

[13] S. D. Kore, J. Imbert, M. J. Worswick, and Y. Zhou, "Electromagnetic impact welding of mg to al sheets," *Sci. Technol. Weld. Joining*, vol. 14, no. 6, pp. 549–553, Aug. 2009, doi: 10.1179/136217109X449201.

[14] S. D. Kore, P. P. Date, and S. V. Kulkarni, "Electromagnetic impact welding of aluminum to stainless steel sheets," *J. Mater. Process. Technol.*, vol. 208, nos. 1–3, pp. 486–493, Nov. 2008, doi: 10.1016/j.jmatprotec.2008.01.039.

[15] S. Hisashi, S. Isao, R. Sherif, and S. Hidekazu, "Numerical study of joining process in magnetic pressure seam welding," *Trans. JWRI*, vol. 38, no. 1, pp. 63–68, 2009.

[16] Z. Fan, H. Yu, and C. Li, "Plastic deformation behavior of bimetal tubes during magnetic pulse cladding: FE analysis and experiments," *J. Mater. Process. Technol.*, vol. 229, pp. 230–243, Mar. 2016, doi: 10.1016/j.jmatprotec.2015.09.021.

[17] J. Cui, Y. Li, Q. Liu, X. Zhang, Z. Xu, and G. Li, "Joining of tubular carbon fiber-reinforced plastic/aluminum by magnetic pulse welding," *J. Mater. Process. Technol.*, vol. 264, pp. 273–282, Feb. 2019, doi: 10.1016/j.jmatprotec.2018.09.018.

[18] E. Thibaudeau and B. L. Kinsey, "Analytical design and experimental validation of uniform pressure actuator for electromagnetic forming and welding," *J. Mater. Process. Technol.*, vol. 215, pp. 251–263, Jan. 2015, doi: 10.1016/j.jmatprotec.2014.08.019.

[19] A. Y. Wu and K. S. Sun, "Formulation and implementation of the current filament method for the analysis of current diffusion and heating in conductors in railguns and homopolar generators," *IEEE Trans. Magn.*, vol. 25, no. 1, pp. 610–615, 1989, doi: 10.1109/20.22610.

[20] L. Shoubao, R. Jiangjun, P. Ying, Z. Yujiao, and Z. Yadong, "Improvement of current filament method and its application in performance analysis of induction coil gun," *IEEE Trans. Plasma Sci.*, vol. 39, no. 1, pp. 382–389, Jan. 2011, doi: 10.1109/TPS.2010.2047276.

HANG ZHANG was born in Zhumadian, Henan, China, in 1990. He is currently pursuing the Ph.D. degree in electrical engineering with the Huazhong University of Science and Technology, Wuhan, China.

His research interests include electromagnetic pulse welding and forming.

QINGJIAN WANG is currently pursuing the Ph.D. degree in electrical engineering with the Huazhong University of Science and Technology, Wuhan, China.

GUANGDA WANG (Member, IEEE) is currently pursuing the Ph.D. degree in electrical engineering with the Huazhong University of Science and Technology, Wuhan, China.

HONGFA DING (Member, IEEE) received the M.S. and Ph.D. degrees from the School of Electrical and Electronic Engineering, Huazhong University of Science and Technology (HUST), Wuhan, China. He is currently a Professor with HUST. His research interests include pulse power technology, high-magnetic field technology, and their application in power systems.